

# UniHead: Unifying Multi-Perception for Detection Heads

Hantao Zhou, Rui Yang, Yachao Zhang, Haoran Duan, Yawen Huang, Runze Hu, Xiu Li,  
Yefeng Zheng, *Fellow, IEEE*

**Abstract**—The detection head constitutes a pivotal component within object detectors, tasked with executing both classification and localization functions. Regrettably, the commonly used parallel head often lacks omni perceptual capabilities, such as deformation perception, global perception and cross-task perception. Despite numerous methods attempting to enhance these abilities from a single aspect, achieving a comprehensive and unified solution remains a significant challenge. In response to this challenge, we develop an innovative detection head, termed UniHead, to unify three perceptual abilities simultaneously. More precisely, our approach (1) introduces deformation perception, enabling the model to adaptively sample object features; (2) proposes a Dual-axial Aggregation Transformer (DAT) to adeptly model long-range dependencies, thereby achieving global perception; and (3) devises a Cross-task Interaction Transformer (CIT) that facilitates interaction between the classification and localization branches, thus aligning the two tasks. As a plug-and-play method, the proposed UniHead can be conveniently integrated with existing detectors. Extensive experiments on the COCO dataset demonstrate that our UniHead can bring significant improvements to many detectors. For instance, the UniHead can obtain +2.7 AP gains in RetinaNet, +2.9 AP gains in FreeAnchor, and +2.1 AP gains in GFL. The code is available at <https://github.com/zht8506/UniHead>.

**Index Terms**—Detection head, Unifying multi-perception, Transformer, Object detection.

## I. INTRODUCTION

Object detection is a fundamental but challenging task that aims to locate and recognize objects of interest in images. Recent years have witnessed remarkable progress in object detection, with advancements in backbone design [1]–[5], feature fusion network optimization [6]–[8], and effective training strategies [9]–[15]. Despite these impressive breakthroughs, the crucial role of detection heads in object detection has not been fully explored in existing research.

The primary purpose of detection heads is to perform accurate classification and localization tasks by utilizing the

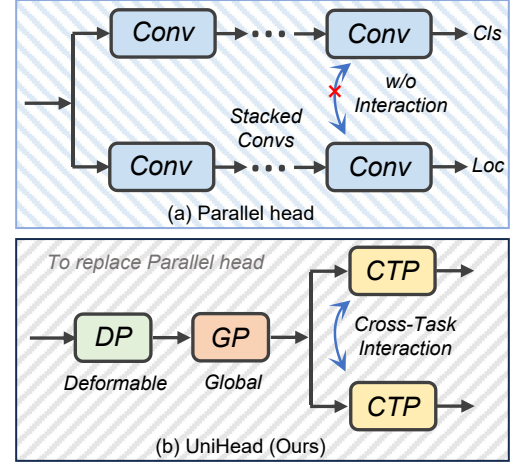


Fig. 1. Overview of the parallel head (a) and our UniHead (b). UniHead integrates *deformation perception* (DP), *global perception* (GP), and *cross-task perception* (CTP) in the detection head.

intricate features extracted from the backbone. One prevalent approach is the parallel head [9], [11], [16], which establishes two isolated branches by employing stacked convolutions to learn task-relevant features, as depicted in Fig. 1(a). However, despite its widespread use, this approach has several limitations, especially the lack of perceptual capabilities necessary for an ideal detector.

In concrete, an ideal detector should possess three critical perceptual capabilities: *deformation perception*, *global perception*, and *cross-task perception*. Specifically, natural objects exhibit two types of diversities: geometric deformation diversity, scale and shape diversity. The former requires the detector can adaptively sample object-relevant features to counter the geometric deformation of the target object (*deformation perception*), while the latter requires *global perception* to capture global features and model long-range dependencies. Additionally, many works [10], [17], [18] have observed that classification predictions and localization predictions may be misaligned, *i.e.*, boxes with high classification scores cannot always be accurately localized. Therefore, the detection head necessitates *cross-task perception* to comprehensively integrate the supervision information from both tasks, thus resulting in consistent detection for classification and localization.

However, the commonly used parallel head [9], [11], [16] cannot provide these perceptions stemming from the convolution properties and the parallel structures. Particularly, the convolution mechanism is limited in both deformation

This work was supported by the National Key R&D Program of China (Grant No.2020AAA0108303), the National Natural Science Foundation of China (No. 62192712), the Shenzhen Science and Technology Project (Grant No.JCYJ20200109143041798) and Shenzhen Stable Supporting Program (WDZC20200820200655001). (Corresponding authors: Runze Hu; Xiu Li.)

Hantao Zhou, Rui Yang, Yachao Zhang, Xiu Li are with Tsinghua Shenzhen International Graduate School, Tsinghua University, Shenzhen, 518055, China (e-mail: hantaozh@outlook.com, r-yang20@mails.tsinghua.edu.cn, yachaozhang@stu.xmu.edu.cn, li.xiu@sz.tsinghua.edu.cn).

Runze Hu is with the School of Information and Electronics, Beijing Institute of Technology, Beijing, 100086, China (e-mail: hrzlpk2015@gmail.com).

Haoran Duan is with the Department of Computer Science, Durham University (E-mail: haoran.duan@ieee.org).

Yawen Huang and Yefeng Zheng are with Tencent Jarvis Lab, Shenzhen, China (E-mail: yawenhuang@tencent.com; yefengzheng@tencent.com).

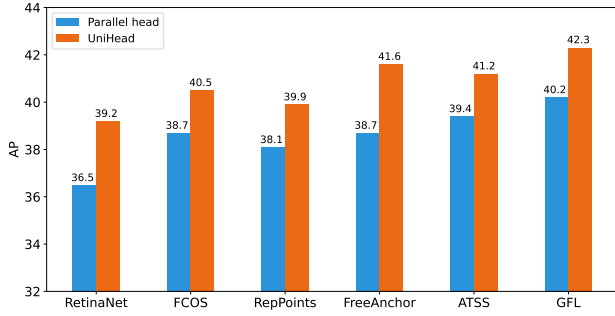


Fig. 2. Our UniHead significantly improves the performance of different detectors, including anchor-based (RetinaNet [9]), anchor-free center-based (FCOS [16]), anchor-free keypoint-based (Reppoints [19]) and strong baseline (FreeAnchor [20], ATSS [11], GFL [10]).

and global perception, as it samples the input feature map at fixed local locations. The parallel structures perform two tasks independently and lack cross-task perception to execute interaction between them, as shown in Fig. 1(a).

Recently, researchers have sought to mitigate the aforementioned issues by proposing novel detection heads. For instance, the dynamic head [21] integrates multiple attentions to unify scale-awareness and spatial-awareness, which alleviates the locality bias of the convolution mechanism. GFL [10] and TOOD [17] combine the supervision information (*e.g.*, classification score and IOU) from both tasks to improve the model’s ability in cross-task perception, thus achieving consistent detection prediction. Double-Head [18] and TSD [22] point out that the feature representations of the classification and regression tasks are different, and propose effective methods to learn task-specific features. Nonetheless, existing approaches are inclined towards enhancing only one of the three perception aspects, lacking a unified approach that can collectively enhance all of these perceptions simultaneously.

In this paper, we thereby propose a plug-and-play detection head, dubbed *UniHead*, to address the above problems from a comprehensive and integrated perspective. UniHead involves different modules to imbue the detector with a comprehensive perceptual capability while not imposing additional computational or architectural burdens. The overall framework of UniHead is presented in Fig. 1(b).

Specifically, we first introduce the deformation perception to UniHead by the classical deformable convolution [23]. This allows the model to sample spatial locations away from local and fixed shapes, resulting in a more effective perception of deformed objects. Second, we propose a Dual-axial Aggregation Transformer (DAT) to model long-range dependencies effectively. DAT performs self-attention on the horizontal and vertical axes in parallel in the channel-compressed space. This design empowers it to capture global information within a single module while maintaining low computational complexity. More importantly, we introduce a Cross-task Interaction Transformer (CIT), which uses cross-attention to facilitate interaction between the classification and localization tasks. By incorporating CIT, UniHead can not only capture the abundant context of one task but also leverage relevant context from the other task, thus explicitly promoting mutual alignment

between the two tasks.

Based on the above three meticulously designed modules, UniHead can effectively enhance multiple perceptual abilities. Our UniHead can be conveniently integrated with existing detectors with ease as a plugin. We conduct extensive experiments on the MS-COCO [24] benchmark to demonstrate the effectiveness of our approach. As shown in Fig. 2, UniHead consistently improves the performance of classical detectors by a large margin. Specifically, when applying UniHead to RetinaNet [9] with ResNet-50 [1] as the backbone, it achieves 39.2 AP and considerably improves the RetinaNet baseline by 2.7 AP. With powerful backbone Swin-B [25] pre-trained on ImageNet-22K dataset [26], our Unihead achieves 54.3 AP, demonstrating the potential of our approach and compatibility with large models. The main contributions of this work can be summarized as follows:

- We propose a novel detection head, namely UniHead, which improves the detection performance by jointly enhancing three essential perceptual abilities of a detector, *i.e.*, deformation perception, global perception and cross-task perception.
- We devise a Dual-axial Aggregation Transformer (DAT) to capture global features effectively and efficiently. Additionally, we introduce a Cross-task Interaction Transformer (CIT) meticulously crafted to facilitate interactions between the classification and localization tasks.
- We have verified various detectors equipped with our method on the MS-COCO benchmark, and results show that our method can constantly improve these detectors by 1.7 ~ 2.9 AP with even fewer computational costs.

## II. RELATED WORK

### A. Object Detection

Recent years have witnessed flourished developments in object detection [9], [16], [27]–[29], with two main categories of object detectors: two-stage and one-stage detectors. Two-stage detectors, such as the R-CNN series [30]–[32], generate region proposals using a Region Proposal Network (RPN) in the first stage and then refine the predictions of these proposals in the second stage. Different from the two-stage paradigm, one-stage detectors eliminate the region proposal step and instead classify and regress the bounding box directly. However, earlier one-stage detectors trailed the detection performance until the emergence of RetinaNet [9], which involves focal loss to solve the class imbalance problem. Following RetinaNet, various detectors eliminate the widely-used anchor and develop anchor-free detectors, which use center [16] and corner points [19] to represent objects. Some researchers also propose novel loss [10] and training strategies [11] to improve the performance of detectors.

### B. Detection Head

The detection head constitutes a pivotal element of a detector, with the widely adopted parallel head being the default choice. However, recent research has unveiled that this standard detection head falls short of achieving optimal detection

performance. For instance, Double-Head [18] suggests that a fully connected head is more suitable for classification tasks, whereas a convolution head is better suited for localization tasks. GFL [10] enriches the concept of a detection head by introducing soft labels. It leverages the IOU score from the localization task as the classification label, forming a joint representation of localization quality and classification. TOOD [17] devises a task-aligned head, designed to strengthen the interaction between classification and localization tasks. Dynamic Head [21] employs attention mechanisms to augment the detection head's perceptual capabilities concerning scale and spatiality. Despite these advancements, current methods tend to address specific subproblems individually. We introduce a comprehensive detection head that enhances the model's detection capabilities from multiple perspectives.

### C. Attention Mechanism

Attention mechanisms hold a critical role in human perception. Inspired by this, they are also widely used in deep learning to boost the performance of the model [33]–[39]. Among various attention mechanisms, deformable convolution [23] can be perceived as a special attention mechanism, which adds a learnable offset to the vanilla convolution to sample spatial locations away from local regions. Recently, Transformers have garnered substantial acclaim in the domain of computer vision, primarily due to their prowess in modeling long-range dependencies [25], [40]–[46]. However, its complexity is quadratic with the image resolution, which limits its application to high-resolution downstream tasks (including object detection). Therefore, plenty of algorithms have been proposed to ameliorate this problem, including introducing global token [47], reducing the spatial size of attention [48], designing novel attention mechanisms (*e.g.*, local-windows attention [25], axial attention [49], criss-cross attention [50], cross-shaped window attention [51]). In this paper, we harness existing attention mechanisms or devise novel ones to augment perceptual capabilities. To minimize the computational overhead, we also incorporate lightweight designs to make our UniHead both effective and efficient.

## III. UNIHEAD

The widely used parallel head [9], [11], [16] fails to effectively cope with two properties of detection tasks: the diversity of objects in nature and the interaction between classification and localization, due to the limitations of convolution and parallel structures. To ameliorate this issue, we propose a novel detection head, termed UniHead, as shown in Fig. 1(b).

UniHead can provide three capabilities for the model: *deformation perception*, *global perception* and *cross-task perception*, in a unified form.

- **Deformation Perception.** Deformation Perception enables the model to learn object-related features adaptively, instead of being trapped in fixed windows and local locations.
- **Global Perception.** Global Perception allows the model to perceive global features and model long-range dependencies, thus detecting objects with various scales more accurately.

- **Cross-Task Perception.** Cross-Task Perception can perform interaction between two tasks to introduce additional supervision information for each task, leading to more consistent prediction.

We leverage or introduce dedicatedly designed modules to achieve these perceptions and unify them to build our UniHead. In general, given a multi-scale feature map, UniHead executes these three modules to catch three perceptions. Then, the output features are employed to perform classification and localization. With this framework, UniHead attempts to unify the three perceptual capabilities in a single head. In the following, we delineate the three perceptions in detail.

### A. Deformation Perception

The objects in natural scenes are complex, with various contents and geometric transformations. The vanilla convolution with a fixed kernel (*e.g.*,  $3 \times 3$ ) fails to tackle this challenging situation well. Thus, inspired by [52], we introduce deformation perception (DP) into the UniHead by using deformable convolution. Deformable convolution can perceive object transformations through learned offsets and scales on multi-scale features. Given a  $3 \times 3$  kernel and offsets  $p_k \in \{(-1, -1), (-1, 0), \dots, (1, 1)\}$ , the deformation learning process at the location  $p$  can be expressed as:

$$X^{DP}(p) = \sum_{k=1}^K W_k \cdot B(X; p + p_k + \Delta p_k) \Delta m_k, \quad (1)$$

where  $K = 9$  donates the number of sampling locations for one  $3 \times 3$  convolution operation and  $W_k$  represents the convolution weights of the  $k$ -th sampling location.  $B(\cdot; \cdot)$  refers to bilinear interpolation on the feature  $X$ .  $\Delta p_k$  and  $\Delta m_k$  denote the predicted offsets and scales at the  $k$ -th sampling location, respectively. The predicted offsets make feature sampling not be restricted to a fixed location, and the modulation scales regulate the importance of each sampling location. With these adaptive sampling offsets and modulation scales, we introduce deformable representation capabilities into the model, thus facilitating the detection of objects with complex shapes and diverse appearances.

### B. Global Perception

Objects with varying scales and shapes often exist in the image, which requires the detector to capture global features to locate their complex boundaries. To address this issue, we propose a Dual-axial Aggregation Transformer (DAT) to model long-range dependencies, resulting in global perception enhancement to detectors. The DAT involves two parts: efficient dual-axial attention and cross-axis aggregation block.

**Efficient Dual-axial Attention.** Although Transformer has demonstrated its effectiveness in global modeling capabilities, its overwhelming computational burden limits its wider range of applications. Alternative methods, such as local window attention [25] and spatial reduction operation [41], [48], often forsake the global capability or lose some spatial information. To overcome these limitations, we propose an Efficient Dual-axial Attention (EDA).

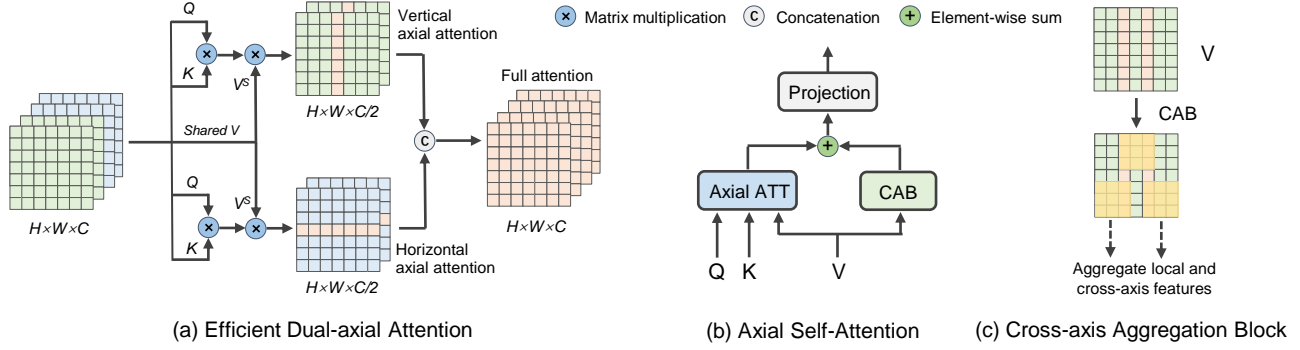


Fig. 3. Illustration of our Dual-axial Aggregation Transformer (DAT). ATT and CAB represent attention and Cross-axis Aggregation Block, respectively.

As shown in Fig. 3(a), the EDA utilizes horizontal and vertical axial attention in parallel to model long-range dependencies. For horizontal axial attention, the input feature  $X \in \mathbb{R}^{H \times W \times C}$  is evenly split into  $H$  non-overlapping horizontal axial stripes, each with  $W$  tokens. Let  $X_i \in \mathbb{R}^{W \times C}$  denotes the  $i$ -th stripe, and the self-attention of  $X_i$  can be formulated as:

$$(Q_i, K_i, V_i^S) = (X_i W_Q, X_i W_K, X_i W_V^S),$$

$$\hat{Y}_i = \text{Attention}(Q_i, K_i, V_i^S) = \text{Softmax}\left(\frac{Q_i K_i^\top}{\sqrt{d_k}}\right) V_i^S, \quad (2)$$

where  $W_Q \in \mathbb{R}^{C \times \frac{C}{2}}$ ,  $W_K \in \mathbb{R}^{C \times \frac{C}{2}}$ ,  $W_V^S \in \mathbb{R}^{C \times \frac{C}{2}}$  represent the projection matrices of queries, keys and values on the input  $X_i$ . Note that channel reduction operation is utilized when calculating queries, keys and values, thus making the attention perform in the channel-compressed space.  $V_i^S$  and  $W_V^S$  represent the shared values and projection matrix and will be used in both horizontal and vertical axial attention.  $d_k$  is the dimension of  $K_i$ .  $\hat{Y}_i \in \mathbb{R}^{W \times C}$  is the horizontal attention output of  $X_i$ . The vertical axial self-attention can be similarly derived and its output is denoted as  $\tilde{Y}$ . Finally, the outputs of two parts are concatenated along the channel dimension. The process is formulated as:

$$\text{EDA}(X) = \text{Cat}(\hat{Y}, \tilde{Y}) W_O, \quad (3)$$

where  $\text{Cat}$  denotes the channel-wise concatenation;  $W_O \in \mathbb{R}^{C \times C}$  is the commonly used projection matrix for feature fusion. The complexity of EDA is:

$$\Omega(\text{EDA}) = HWC \times (3.5C + H + W). \quad (4)$$

Thus, the EDA reduces the complexity of attention to be quadratic to image height or width ( $O(H^2)$  or  $O(W^2)$ ), rather than to the image resolution ( $O((HW)^2)$ ).

Compared with other axial strip-like attention mechanisms, *e.g.*, axial attention [49], criss-cross attention [50] and Seaformer block [53], the proposed EDA demonstrates several unique advantages. Specifically, our EDA is computed in the channel compressed space and shares the same value map for vertical and horizontal axial attention. These properties enable EDA to efficiently capture global features in a single layer instead of stacking more self-attention layers as axial attention and criss-cross attention. Hence, our EDA is more flexible to

various vision tasks. Furthermore, in contrast to the Seaformer block, EDA does not require squeezing the axial features, thereby ensuring a more comprehensive retention of spatial information. Ablation experiments (Table VI) demonstrate the superiority of our method.

**Cross-axis Aggregation Block.** Although the EDA can effectively model long-range dependencies between tokens, it falls short in learning local information due to the lack of inductive bias of self-attention. In addition, axial attention cannot aggregate cross-axis information directly. In order to complement the EDA with the locality and achieve global and local coupling, we propose a cross-axis aggregation block (CAB). As illustrated in Fig. 3(b), the CAB is applied on the value ( $V$ ) map and operates in parallel to the axial attention. Formulaically, this process can be expressed as:

$$\hat{Z} = \hat{Y} + \text{CAB}(\hat{V}), \quad (5)$$

where  $\hat{V}$  and  $\hat{Z}$  denote the value map and output of horizontal axial attention, respectively. The function of CAB can be easily implemented by a  $3 \times 3$  depth-wise convolution. CAB offers a more flexible mechanism that not only provides attention with positional information but also enables interaction and aggregation among different axial stripe-like attentions, as depicted in Fig. 3(c).

With the proposed EDA and CAB, our Dual-axial Aggregation Transformer (DAT) can effectively model long-range dependencies and achieve global perception, thus performing more precise localization.

### C. Cross-Task Perception

Object detection is the integration of classification and localization. The detection head is required to utilize information from both tasks to make consistent predictions, rather than executing the two tasks independently. Namely, the detector is required to output the box with precise location and high classification confidence. Thus, we propose a Cross-task Interaction Transformer (CIT) that compensates for the model's ability to perform cross-task interaction. As shown in Fig. 4, the CIT possesses two significant components: cross-task channel-wise attention and locality enhancement block.

**Cross-task Channel-wise Attention.** We leverage channel-wise cross-attention to perform interaction between classification and localization tasks. Channel-wise attention can benefit



the model from two aspects: (1) reduce the complexity of attention to be linear with the image size; (2) enhance the channel-wise global perception for the model while being complementary with DAT that focuses on global spatial-wise perception. And the cross-attention empowers the model to leverage features from one task to inform and guide the feature learning process of another task.

Specifically, prior to feeding features into CIT, we first utilize conditional positional encoding [54] to encode position information for classification and localization features, and the outputs denote  $X^c \in \mathbb{R}^{(H \times W) \times C}$  and  $X^l \in \mathbb{R}^{(H \times W) \times C}$ , respectively. As shown in the left side of Fig. 4, when CIT is applied to the classification branch, the Cross-task Channel-wise Attention (CCA) can be described as:

$$\begin{aligned} (K^c, V^c) &= (X^c W_K^c, X^c W_V^c), \\ (K^l, V^l) &= (X^l W_K^l, X^l W_V^l), \\ Q &= X^l W_Q^l, K = \text{Cat}(K^c, K^l), V = \text{Cat}(V^c, V^l), \quad (6) \\ CCA(X^c, X^l) &= CA(Q, K, V) = V \text{Softmax}\left(\frac{Q^\top K}{\sqrt{d_k}}\right), \end{aligned}$$

where  $W_K^c, W_V^c, W_K^l$  and  $W_V^l \in \mathbb{R}^{C \times \frac{C}{2}}$  are the projection matrices of keys and values for the input  $X^c$  and  $X^l$ , respectively;  $W_Q^l \in \mathbb{R}^{C \times C}$  denotes the projection matrix of queries for the input  $X^l$ ;  $CA$  represents the channel-wise attention that calculates attention among channels.

As shown in Equation 6, we use the cross-task supervision information from  $X^l$  as queries to guide the representation learning of classification feature  $X^c$ . Furthermore, we concatenate the features of two tasks to generate keys and values. The attention weight can be obtained as in  $Q^\top K = \text{Cat}(Q^\top K^c, Q^\top K^l)$ , and thus the outputs of CIT can perceive the features of two tasks. As a result, the representation learning of one task (e.g., localization task) will be guided by the information of another task (e.g., classification task). With this cross-interaction design, the model will consider both localization accuracy and classification confidence to produce detection results that are consistent with the two tasks. Ablation experiments show (Table IX) that the attention with cross-task information interaction can achieve superior performance, without adding any parameter and computation.

Compared with other cross-attention modules, such as the deep fusion employed in GLIP [55], our CIT module operates within the context of localization and classification tasks to facilitate mutual guidance between the two tasks. In contrast, GLIP primarily focuses on cross-modal interaction between images and text. Furthermore, for each attention branch, our CIT concatenates the key and value features of the two branches as the  $K$  and  $V$  of attention, while GLIP directly employs the features of the other branch as the  $K$  and  $V$ .

**Locality Enhancement Block.** Since channel-wise attention lacks the ability to learn local spatial-wise features, we propose a locality enhancement block (LEB) to alleviate this problem. The LEB is lightweight and effective, which builds on depth-wise convolutions with different kernel sizes. Formulaically, it can be described as:

$$LEB(X^{CCA}) = DW_{1 \times 1}(DW_{3 \times 3}(DW_{1 \times 1}(X^{CCA}))), \quad (7)$$

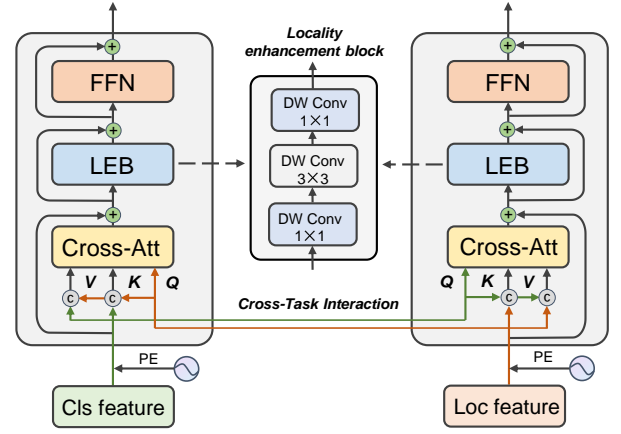


Fig. 4. Illustration of the proposed Cross-task Interaction Transformer. PE denotes the positional encoding process.

where  $DW$  denotes the depth-wise convolution;  $X^{CCA}$  represents the features output from cross-task channel-wise attention (CCA). The two  $1 \times 1$  depth-wise convolutions can further modulate the importance of each channel, which are channel-wise scales. The  $3 \times 3$  depth-wise convolution can learn locality information and compensate inductive bias for the model.

So far, three perception modules have been illustrated in detail. These modules are connected in series to form our UniHead, which yields absolute gains on both object detection (Table I) and instance segmentation (Table XII) tasks.

## IV. EXPERIMENTS

### A. Dataset and Evaluation Metrics

We evaluate our approach on the two classical benchmarks, i.e., MS-COCO [24] and PASCAL VOC [56]. Specifically, MS-COCO dataset has 80 object categories of around 164K images, with 118k images for training, 5k images for validation and 41k images for testing. We train our model on *train2017* subset and evaluate the performances on the *val2017* subset for ablation study and on *test-dev* subset for comparison with state-of-the-art methods. PASCAL VOC contains two representative sets, i.e., VOC2007 and VOC2012, with 20 object categories. We use the trainval set of VOC2007 and VOC2012 (16551 images) for training and the test set of VOC2007 (4952 images) for testing, denoted as VOC07+12.

The detection performance is measured by the standard COCO-style Average Precision (AP) metrics for COCO dataset and standard mean Average Precision (mAP) metrics for VOC dataset. We employ Params and GFLOPs to evaluate the model efficiency, which represent the number of parameters and floating point operations of the model, respectively.

### B. Implementation Details

We employ our UniHead as a plugin to replace the default parallel head in different classical detectors. We implement our method based on the popular mmdetection [57] and use the models pre-trained on the ImageNet [26] dataset as the backbone. We adopt AdamW as the optimizer with an initial

TABLE I  
RESULTS OF APPLYING UNIHEAD TO DIFFERENT CLASSICAL DETECTORS ON COCO *val*2017.

Detector	Note	#Param.	FLOPs	AP	AP <sub>50</sub>	AP <sub>75</sub>	AP <sub>S</sub>	AP <sub>M</sub>	AP <sub>L</sub>
<i>Anchor-based</i>									
RetinaNet [9]	baseline	37.74M	239.32G	36.5	55.4	39.1	20.4	40.3	48.1
RetinaNet [9]	UniHead	37.34M	239.12G	<b>39.2 (+2.7)</b>	<b>59.7</b>	<b>41.7</b>	<b>23.6</b>	<b>43.0</b>	<b>51.1</b>
<i>Anchor-free</i>									
FCOS [16]	baseline	32.02M	200.55G	38.7	57.4	41.8	22.9	42.5	50.1
FCOS [16]	UniHead	31.61M	200.31G	<b>40.4 (+1.7)</b>	<b>59.8</b>	<b>43.7</b>	<b>24.7</b>	<b>43.8</b>	<b>52.3</b>
<i>Keypoint-based</i>									
RepPoints [19]	baseline	36.62M	218.07G	38.1	58.7	40.8	22.0	41.9	50.1
RepPoints [19]	UniHead	37.40M	243.02G	<b>39.9 (+1.8)</b>	<b>60.7</b>	<b>42.7</b>	<b>24.0</b>	<b>43.6</b>	<b>53.0</b>
<i>Strong Baseline</i>									
FreeAnchor [20]	baseline	37.74M	239.32G	38.7	57.3	41.5	21.0	42.0	51.3
FreeAnchor [20]	UniHead	37.34M	239.12G	<b>41.6 (+2.9)</b>	<b>61.5</b>	<b>45.0</b>	<b>24.3</b>	<b>45.2</b>	<b>54.8</b>
ATSS [11]	baseline	32.07M	205.30G	39.4	57.6	42.8	23.6	42.9	50.3
ATSS [11]	UniHead	31.66M	205.06G	<b>41.2 (+1.8)</b>	<b>59.9</b>	<b>45.1</b>	<b>25.3</b>	<b>44.9</b>	<b>53.7</b>
GFL [10]	baseline	32.22M	208.39G	40.2	58.4	43.3	23.3	44.0	52.2
GFL [10]	UniHead	31.81M	208.16G	<b>42.3 (+2.1)</b>	<b>61.1</b>	<b>45.6</b>	<b>24.5</b>	<b>46.0</b>	<b>55.3</b>

learning rate of 0.0001 and a weight decay of 0.2. A warmup strategy is employed to stabilize the training for the first 500 steps, which is the default strategy in mmdetection. When training 12 epochs, the learning rate decreased by a factor of 0.1 after 9-th and 11-th epochs. All experiments are performed on 8 V100 GPUs each with 32GB memory.

### C. Main Results

We first replace the parallel head with our UniHead in different popular detectors to evaluate the effectiveness of our approach. We then integrate the UniHead with a range of different backbones to demonstrate the compatibility and versatility of our method.

**Applying to classical detectors.** We evaluate the effectiveness and generalization ability of the UniHead by plugging it into popular object detectors, including RetinaNet [9], FCOS [16], RepPoints [19], FreeAnchor [20], ATSS [11] and GFL [10]. These selected detectors represent a wide range of object detection frameworks, including anchor-based, anchor-free center-based, anchor-free keypoint-based and strong baseline (improved version of existing works). To ensure a fair comparison, we used a perception module number configuration of 1, 2, 2 to maintain a comparable complexity to the parallel head. The results are reported in Table I. Note Reppoints has fewer convolutions in the parallel head than the other selected detectors, so the complexity of our method is slightly higher. As shown in Table I, UniHead consistently improves the performance of all detectors by notable margins, such as 2.7 AP improvement on RetianNet and 2.9 AP improvement on FreeAnchor, with even fewer parameters and computations. These results illustrate the effectiveness and efficiency of our method.

**Cooperating with Different Backbones.** We demonstrate the compatibility of our approach with various backbones and compare it with state-of-the-art (SOTA) detectors. We leverage GFLv2 [58] as our detection framework with a number of perception modules of 1, 3, 3. We adopt multi-scale training strategy during training and test our model on a single scale.

For a fair comparison, we report the results of other models using multi-scale training and single scale testing.

As shown in Table II, our UniHead consistently achieves impressive performance with various backbones and surpasses the counterpart SOTA model by a large margin. Specifically, when compared to the recent detector DDOD [60], with the same settings, our method outperforms it by 0.7 AP with the ResNet-101 backbone. Additionally, our method demonstrates notably enhanced learning efficiency, *e.g.*, it achieves an improvement of 1.6 AP over DDQ FCN [62] with fewer training epochs (24 v.s. 36 epochs) when utilizing ResNeXt-101 as the backbone. Compared with the DETR series [42], [61], [66], our UniHead achieves higher accuracy with fewer training epochs (24 v.s. 50 epochs). Our UniHead is also compatible with Transformer-based backbone (Swin-T [25]) and outperforms excellent Cascade Mask R-CNN [32] by 0.9 AP. Moreover, we use Swin-B pre-trained on ImageNet-22K dataset [26] as the backbone to explore the performance improvements with large models. As shown in Table II, with a stronger pre-trained backbone, our UniHead achieves a tremendous performance improvement to 54.3 AP, demonstrating the potential for further improvements of our method.

### D. Ablation Study

We perform comprehensive ablations to demonstrate the effectiveness and efficiency of our UniHead. For the ablation study, UniHead is applied to RetinaNet with ResNet-50 backbone and trained for 12 epochs without multi-scale training.

**Effectiveness of Perception Modules.** To evaluate the effectiveness of each proposed module, we conduct a controlled study in which we *eliminate* the parallel head used in RetinaNet and gradually add different perception modules to it. The results of the study are presented in Table III. Our findings indicate that when only one perception is applied to RetinaNet, it fails to achieve satisfactory results. Interestingly, we observe that the use of cross-task perception alone outperforms the baseline, underscoring the significance of cross-task interaction. With the addition of more perception modules, we observe an impressive enhancement in RetinaNet’s performance.

TABLE II

COMPARISON WITH RESULTS USING DIFFERENT BACKBONES ON COCO *test-dev*. THE RESULTS ARE ARRANGED IN THE INCREASING ORDER OF AP. <sup>†</sup> REPRESENTS THAT THE MODEL IS PRE-TRAINED ON THE LARGE IMAGENET-22K DATASET.

Method	Backbone	Val/Test	Epochs	AP	AP <sub>50</sub>	AP <sub>75</sub>	AP <sub>S</sub>	AP <sub>M</sub>	AP <sub>L</sub>	Reference
ATSS [11]	ResNet-50	val	12	39.3	57.5	42.8	24.3	43.3	51.3	CVPR20
GFLV2 [58]	ResNet-50	val	12	41.1	58.8	44.9	23.5	44.9	53.3	CVPR21
Cascade Mask R-CNN [32]	ResNet-50	val	12	41.3	59.4	45.3	23.2	43.8	55.8	CVPR18
DW [59]	ResNet-50	val	12	41.5	59.8	45.0	-	-	-	CVPR22
ATSS-DDOD [60]	ResNet-50	val	12	42.0	60.0	45.4	26.2	45.4	53.7	TMM
TOOD [17]	ResNet-50	val	12	42.5	59.8	46.4	-	-	-	ICCV21
DyHead [21]	ResNet-50	val	12	42.6	60.1	46.4	-	-	-	CVPR21
<b>UniHead</b>	ResNet-50	val	12	<b>42.8</b>	61.0	46.2	24.8	46.8	56.8	TNNLS
Cascade R-CNN [32]	ResNet-101	test-dev	36	42.8	62.1	46.3	23.7	45.5	55.2	CVPR18
DAB-DETR [61]	ResNet-101	val	50	43.5	63.9	46.6	23.6	47.3	61.5	ICLR22
ATSS [11]	ResNet-101	test-dev	24	43.6	62.1	47.4	26.1	47.0	53.6	CVPR20
HSD [13]	ResNet-101	test-dev	160	44.2	63.9	49.0	26.2	48.5	55.2	TNNLS
DN-DETR [42]	ResNet-101	val	50	45.2	65.5	48.3	24.1	49.1	65.1	CVPR22
DDQ FCN [62]	ResNet-101	test-dev	24	45.9	65.1	50.7	28.3	48.6	55.6	CVPR23
RepPoints v2 [63]	ResNet-101	test-dev	24	46.0	65.3	49.5	27.4	48.9	57.3	NeurIPS20
GFLV2 [58]	ResNet-101	test-dev	24	46.2	64.3	50.5	27.8	49.9	57.0	CVPR21
DyHead [21]	ResNet-101	test-dev	24	46.5	64.5	50.7	28.3	50.3	57.5	CVPR21
TOOD [17]	ResNet-101	test-dev	24	46.7	64.6	50.7	28.9	49.6	57.0	ICCV21
DDOD [60]	ResNet-101	test-dev	24	47.0	65.3	51.3	30.2	50.4	57.2	TMM
<b>UniHead</b>	ResNet-101	test-dev	24	<b>47.7</b>	66.3	52.1	28.9	51.2	59.0	TNNLS
ATSS [11]	ResNeXt-101-64x4d	test-dev	24	45.6	64.6	49.7	28.5	48.9	55.6	CVPR20
Sparse R-CNN [64]	ResNeXt-101-64x4d	test-dev	36	46.9	66.3	51.2	28.6	49.2	58.7	CVPR21
Gao <i>et al</i> [65]	ResNeXt-101-64x4d	test-dev	24	47.2	66.7	51.4	29.4	50.4	58.2	TCSVT
DDQ FCN [62]	ResNeXt-101-64x4d	test-dev	36	47.7	67.0	52.6	30.4	49.9	58.3	CVPR23
DyHead [21]	ResNeXt-101-64x4d	test-dev	24	47.7	65.7	51.9	31.5	51.7	60.7	CVPR21
DW [59]	ResNeXt-101-64x4d	test-dev	24	48.2	67.1	52.2	29.6	51.2	60.8	CVPR22
TOOD [17]	ResNeXt-101-64x4d	test-dev	24	48.3	66.5	52.4	30.7	51.3	58.6	ICCV21
Deformable DETR [66]	ResNeXt-101-64x4d	test-dev	50	49.0	68.5	53.2	29.7	51.7	62.8	ICLR21
<b>UniHead</b>	ResNeXt-101-64x4d	test-dev	24	<b>49.3</b>	68.2	53.8	30.8	52.8	60.8	TNNLS
Mask R-CNN [67]	Swin-T	test-dev	36	46.0	68.1	50.3	31.2	49.2	60.1	ICCV17
ATSS [68]	Swin-T	test-dev	36	47.2	66.5	51.3	-	-	-	CVPR20
Sparse R-CNN [64]	Swin-T	test-dev	36	47.9	67.3	52.3	-	-	-	CVPR21
RecursiveDet [69]	Swin-T	test-dev	36	49.1	68.5	53.9	30.5	51.2	61.9	ICCV23
DyHead [21]	Swin-T	test-dev	24	49.7	68.0	54.3	33.3	54.2	64.2	CVPR21
Dy-Mask R-CNN [21]	Swin-T	val	24	49.9	-	-	-	-	-	CVPR23
RepPoints v2 [63]	Swin-T	test-dev	36	50.0	68.6	53.7	33.3	53.6	65.1	NeurIPS20
Mask RepPoints v2 [63]	Swin-T	test-dev	36	50.4	69.3	54.6	33.5	53.8	66.0	NeurIPS20
Cascade Mask R-CNN [32]	Swin-T	test-dev	36	50.4	69.2	54.7	33.8	54.1	65.2	CVPR18
<b>UniHead</b>	Swin-T	test-dev	36	<b>51.3</b>	70.1	56.1	32.5	54.5	64.3	TNNLS
<b>UniHead</b>	Swin-B <sup>†</sup>	test-dev	36	<b>54.3</b>	73.2	59.1	35.1	57.8	68.5	TNNLS

TABLE III

ABLATION STUDY ON THE EFFECTIVENESS OF EACH PERCEPTION MODULE. TWO ✓ REPRESENT REPEATEDLY STACKING ONE MODULE.

DP	GP	CTP	#Param.	FLOPs	AP	AP <sub>50</sub>	AP <sub>75</sub>
Baseline			37.74M	239.32G	36.5	55.4	39.1
✓	×	×	33.67M	152.60G	34.3	54.9	36.9
×	✓	×	34.54M	173.49G	35.8	56.8	38.0
×	×	✓	35.17M	190.41G	36.6	56.9	38.6
✓✓	×	×	34.98M	180.42G	36.2	56.5	38.7
×	✓✓	×	36.06M	204.32G	37.3	58.1	39.6
×	×	✓✓	36.24M	216.27G	37.5	58.3	39.7
×	✓	✓	36.69M	225.21G	37.9	58.3	40.1
✓	×	✓	35.82M	204.32G	38.0	58.4	40.3
✓	✓	×	35.19M	187.40G	37.9	58.9	40.9
✓	✓	✓	37.34M	239.12G	<b>39.2</b>	<b>59.7</b>	<b>41.7</b>

For instance, when both global and cross-task perception are utilized, our UniHead surpasses the baseline by 1.4 AP, *even with much lower computational complexity*. Furthermore, we conduct experiments to repeatedly stack a module multiple times instead of stacking two different modules, as shown in the middle part of Table III. We observe that repeated stacking of one module improves the model performance (*e.g.*, row 3 *v.s.* row 6). However, it is noteworthy that this improvement fails to surpass the performance achieved through the stacking of two different modules, even with higher model complexity (*e.g.*, row 7 *v.s.* row 11). This clearly demonstrates that there are complementary effects between the different modules that can synergistically improve the model performance. Finally, our full UniHead that integrates three perceptual capabilities significantly improves the baseline by 2.7 AP.

**Number of Perception Modules.** We evaluate the efficiency and scalability of our method by stacking different numbers of perception modules. The deformation perception

TABLE IV  
PERFORMANCE OF STACKING DIFFERENT NUMBERS OF PERCEPTION  
MODULES IN OUR UNIHEAD.

DConv	DAT	CIT	#Param.	FLOPs	AP	AP <sub>50</sub>	AP <sub>75</sub>
Baseline			37.74M	239.32G	36.5	55.4	39.1
1	1	1	35.51M	195.86G	38.2	58.8	40.8
1	2	2	37.34M	239.12G	39.2	59.7	41.7
1	3	3	39.17M	282.38G	39.8	60.2	<b>42.6</b>
1	4	4	41.00M	325.64G	<b>39.9</b>	<b>60.5</b>	42.4

TABLE V  
EFFECTIVENESS OF THE DEFORMATION PERCEPTION.

Method	#Param.	FLOPs	AP	AP <sub>50</sub>	AP <sub>75</sub>
Conv	37.28M	237.79G	38.8	59.1	<b>42.1</b>
DConv	37.34M	239.12G	<b>39.2</b>	<b>59.7</b>	41.7

TABLE VI  
COMPARISON WITH OTHER TRANSFORMER MODULES.

Method	#Param.	FLOPs	AP	AP <sub>50</sub>	AP <sub>75</sub>
CCNet Block [50]	37.04M	232.96G	38.7	59.0	41.3
Swin Block [25]	37.40M	240.10G	38.8	59.3	41.4
CSwin Block [51]	37.40M	259.82G	38.9	59.6	41.3
Axial Attention [49]	37.40M	240.36G	38.9	59.4	41.7
DAT (Ours)	<b>37.34M</b>	<b>239.12G</b>	<b>39.2</b>	<b>59.7</b>	<b>41.7</b>

module can be regarded as an implicit position encoding [54], and therefore, we keep its number at 1. As indicated in Table IV, our method can consistently gain considerable performance improvements by stacking more modules until the number of modules reaches 1, 4, 4. Notably, even with much lower complexity, our method, which employs one module per perception type, can significantly outperform the baseline by 1.7 AP. It demonstrates the efficiency of our method. Moreover, when we adopt the model configuration of 1, 3, 3, the UniHead achieves 39.8 AP, which significantly improves the baseline by 3.3 AP, illustrating the powerfulness and scalability of our method.

**Effectiveness of Deformation Perception.** We evaluate the effectiveness of deformation perception by replacing the deformable convolution (DConv) with a standard  $3 \times 3$  convolution (Conv). As reported in Table V, the deformable convolution outperforms the vanilla convolution by 0.4 AP. This suggests that the deformation perception can boost the model’s representation ability and detection performance.

**Comparison with other Transformer modules.** We compare the Dual-axial Aggregation Transformer (DAT) with other classical Transformer modules, including CCNet block [50], Swin-Transformer block [25], CSwin-Transformer block [51] and axial attention [49]. We replace the DAT with these Transformer modules while maintaining the other structures unchanged for a fair comparison. The results are reported in Table VI. We observe that the model equipped with CCNet block has a comparable performance with the least amount of parameters and calculations. Nevertheless, our DAT achieves the optimal trade-off between efficiency and accuracy.

TABLE VII  
ABLATION ON DIFFERENT STRIPE WIDTHS IN THE GLOBAL PERCEPTION  
MODULE.

Stripe width	#Param.	FLOPs	AP	AP <sub>50</sub>	AP <sub>75</sub>
1	37.34M	239.12G	<b>39.2</b>	<b>59.7</b>	<b>41.7</b>
3	37.34M	245.70G	38.9	59.4	41.4
5	37.34M	248.96G	38.8	59.3	41.6

TABLE VIII  
EFFECT OF THE CROSS-AXIS AGGREGATION BLOCK (CAB) IN THE  
CROSS-TASK INTERACTION TRANSFORMER (CIT).

CAB	#Param.	FLOPs	AP	AP <sub>50</sub>	AP <sub>75</sub>
	37.34M	239.01G	39.0	59.7	41.5
✓	37.34M	239.12G	<b>39.2</b>	59.7	<b>41.7</b>

TABLE IX  
EFFECTIVENESS OF THE CROSS-TASK INTERACTION.

Method	#Param.	FLOPs	AP	AP <sub>50</sub>	AP <sub>75</sub>
CSA	37.34M	239.12G	38.9	59.7	41.4
CCA	37.34M	239.12G	<b>39.2</b>	59.7	<b>41.7</b>

TABLE X  
EFFECT OF THE LOCALITY ENHANCEMENT BLOCK (LEB) IN THE  
CROSS-TASK PERCEPTION MODULE.

LEB	#Param.	FLOPs	AP	AP <sub>50</sub>	AP <sub>75</sub>
	37.31M	238.46G	39.0	59.5	<b>41.8</b>
✓	37.34M	239.12G	<b>39.2</b>	<b>59.7</b>	41.7

**Stripe width.** Table VII presents an ablation analysis of the stripe width in the CIT module. The results reveal that the expansion of the attention area does not lead to further improvements in the model’s performance; in fact, it may even cause a decline in its performance. This indicates that the potency of the DAT is derived from its efficient parallel structure, which allows the model to perceive global information.

**Effectiveness of Cross-axis Aggregation Block.** Table VIII presents the results of employing the cross-axis aggregation block (CAB) in the CIT module. CAB effectively integrates both local and cross-axis information for horizontal and vertical axial attention, thus gaining performance improvement.

**Effectiveness of Cross-Task Perception.** To evaluate the effect of cross-task perception, we replace the cross-task channel-wise attention (CCA) with channel-wise self-attention (CSA). As shown in Table IX, the CCA outperforms the CSA by 0.3 AP, without adding additional parameters and computations. This indicates that incorporating cross-task information can effectively guide feature learning for classification and localization tasks, thus achieving higher performance.

**Effectiveness of Locality Enhancement Block.** We ablate the locality enhancement block (LEB) in the cross-task perception module. As shown in Table X, the proposed LEB is lightweight and improves the model by 0.2 AP, proving the significance of the locality enhancement.





Fig. 5. Visualization of detection results of RetinaNet with parallel head and RetinaNet with UniHead. With our UniHead, the model is capable of more effectively detecting objects with diverse deformations and scales, and it can produce high-confidence precise bounding boxes. The major difference is marked by the orange circle. Zoom in for a better view.



Fig. 6. Visualization of failure cases of RetinaNet with our UniHead. Our method encounters challenges in detecting objects that are heavily occluded or concealed. The major difference is marked by the orange circle. Zoom in for a better view.

### E. Visualization

We visualize the detection results using RetinaNet and after replacing its parallel head with UniHead. As shown in Fig. 5, UniHead can detect objects in complex scenes more effectively, where the objects have various scales and diverse geometric transformations. Notably, the third column of the figure highlights UniHead’s proficiency in detecting small objects effectively. This excellent detection performance, particularly for complex-shaped and small objects, underscores the efficacy of deformation perception and global perception. Furthermore, as depicted in the last column of Fig. 5, our method can provide precise detection boxes with higher classification scores, indicating that UniHead can help the detector output more consistent results in both classification and localization.

Furthermore, we visualize the failure cases of RetinaNet with our UniHead in Fig. 6. We can notice that our UniHead faces challenges in detecting objects under conditions of heavy

occlusion or concealment. This may be attributed to that our current approach does not explicitly incorporate mechanisms to handle such scenarios. Future work will explore how to enhance our UniHead so as to better cope with this challenge.

### F. Generalization Capability Verification

To evaluate the generalization capability of our UniHead, we apply our method to another dataset, *i.e.*, VOC dataset [56], as well as the two-stage detectors.

**Applying to VOC dataset.** We apply our UniHead to various typical detectors and evaluate the performance on VOC dataset. Table XI demonstrates the experimental results. It can be noticed that our method consistently improves the detection performance on various detectors significantly, such as 1.7 mAP improvement on RetinaNet and 2.0 mAP improvement on FreeAnchor. These results indicate that our UniHead can be effectively used to other datasets, validating the powerful generalization capability of our method.

TABLE XI

RESULTS OF APPLYING UNIHEAD TO DIFFERENT CLASSICAL DETECTORS ON VOC07+12 DATASET.

Detector	Note	#Param.	FLOPs	mAP
<b>Anchor-based</b>				
RetinaNet [9]	baseline	36.49G	211.78G	78.8
RetinaNet [9]	UniHead	36.09G	211.58G	<b>80.5 (+1.7)</b>
<b>Anchor-free</b>				
FCOS [16]	baseline	31.88M	197.60G	78.2
FCOS [16]	UniHead	31.47M	197.36G	<b>79.6 (+1.4)</b>
<b>Keypoint-based</b>				
RepPoints [19]	baseline	36.60M	217.74G	80.2
RepPoints [19]	UniHead	37.38M	242.69G	<b>81.8 (+1.6)</b>
<b>Strong Baseline</b>				
FreeAnchor [20]	baseline	36.49M	212.78G	79.3
FreeAnchor [20]	UniHead	36.09M	212.58G	<b>81.3 (+2.0)</b>
ATSS [11]	baseline	31.93M	202.35G	79.4
ATSS [11]	UniHead	31.52M	202.11G	<b>80.4 (+1.0)</b>
GFL [10]	baseline	32.08M	205.44G	79.5
GFL [10]	UniHead	31.67M	205.21G	<b>81.0 (+1.5)</b>

TABLE XII

APPLYING UNIHEAD TO TWO-STAGE MODELS FOR OBJECT DETECTION (BBOX) AND INSTANCE SEGMENTATION (SEGM).

Detector	Note	Task	AP	AP <sub>50</sub>	AP <sub>75</sub>
Faster R-CNN [31]	baseline	BBox	37.4	58.1	40.4
Faster R-CNN [31]	UniHead	BBox	<b>39.0</b>	<b>59.7</b>	<b>42.5</b>
Mask R-CNN [67]	baseline	Segm	34.7	55.7	37.2
Mask R-CNN [67]	UniHead	Segm	<b>35.8</b>	<b>56.6</b>	<b>38.3</b>

**Applying to two-stage detectors.** We further generalize our UniHead to representative two-stage models on two scenes, including object detection using Faster R-CNN [31] and instance segmentation using Mask R-CNN [67]. Although two-stage models do not have the parallel head, our UniHead can be easily integrated into them. We use our UniHead to replace the convolution before performing proposal prediction in the Region Proposal Network (RPN). Note the convolution number in RPN is one, so UniHead is used after channel reduction to avoid increasing much complexity. As shown in Table XII, our model still achieves very stunning performance on these scenarios. Specifically, the UniHead improves Faster R-CNN by 1.6 AP and Mask R-CNN by 1.1 AP, fully validating the generalization ability of our approach.

## V. CONCLUSION

In this paper, we propose UniHead, a novel approach that unifies deformation perception, global perception, and cross-task perception in a single head. Firstly, we introduce the deformation perception, which allows the model to adaptively sample the features of objects. Secondly, we design an innovative Dual-axial Aggregation Transformer (DAT) to learn global features effectively. Lastly, we develop the Cross-task Interaction Transformer (CIT), which enables interaction between classification and localization tasks to promote the alignment of the two tasks. As a plugin block, our UniHead can be flexibly integrated into existing object detectors and significantly enhance their performance without adding any model complexity.

## REFERENCES

- [1] K. He, X. Zhang, S. Ren, and J. Sun, "Deep residual learning for image recognition," in *Proc. CVPR*, 2016, pp. 770–778.
- [2] C.-Y. Wang, H.-Y. M. Liao, Y.-H. Wu, P.-Y. Chen, J.-W. Hsieh, and I.-H. Yeh, "Cspnet: A new backbone that can enhance learning capability of cnn," in *Proc. CVPRW*, 2020, pp. 390–391.
- [3] M. Tan, R. Pang, and Q. V. Le, "Efficientdet: Scalable and efficient object detection," in *Proc. CVPR*, 2020, pp. 10781–10790.
- [4] A. Xiao, B. Shen, J. Tian, and Z. Hu, "Pp-nas: Searching for plug-and-play blocks on convolutional neural networks," *IEEE Trans. Neural Netw. Learn. Syst.*, 2023.
- [5] H. Zhou, R. Yang, R. Hu, C. Shu, X. Tang, and X. Li, "Etdnet: Efficient transformer-based detection network for surface defect detection," *IEEE Trans. Instrum. Meas.*, 2023.
- [6] T.-Y. Lin, P. Dollár, R. Girshick, K. He, B. Hariharan, and S. Belongie, "Feature pyramid networks for object detection," in *Proc. CVPR*, 2017, pp. 2117–2125.
- [7] S. Liu, L. Qi, H. Qin, J. Shi, and J. Jia, "Path aggregation network for instance segmentation," in *Proc. CVPR*, 2018, pp. 8759–8768.
- [8] G. Ghiasi, T.-Y. Lin, and Q. V. Le, "Nas-fpn: Learning scalable feature pyramid architecture for object detection," in *Proc. CVPR*, 2019, pp. 7036–7045.
- [9] T.-Y. Lin, P. Goyal, R. Girshick, K. He, and P. Dollár, "Focal loss for dense object detection," in *Proc. ICCV*, 2017, pp. 2980–2988.
- [10] X. Li, W. Wang, L. Wu, S. Chen, X. Hu, J. Li, J. Tang, and J. Yang, "Generalized focal loss: Learning qualified and distributed bounding boxes for dense object detection," in *Proc. NIPS*, vol. 33, 2020, pp. 21002–21012.
- [11] S. Zhang, C. Chi, Y. Yao, Z. Lei, and S. Z. Li, "Bridging the gap between anchor-based and anchor-free detection via adaptive training sample selection," in *Proc. CVPR*, 2020, pp. 9759–9768.
- [12] Z. Ge, S. Liu, Z. Li, O. Yoshie, and J. Sun, "Ota: Optimal transport assignment for object detection," in *Proc. CVPR*, 2021, pp. 303–312.
- [13] J. Cao, Y. Pang, J. Han, and X. Li, "Hierarchical regression and classification for accurate object detection," *IEEE Trans. Neural Netw. Learn. Syst.*, 2021.
- [14] M. Mao, Y. Tian, B. Zhang, Q. Ye, W. Liu, and D. Doermann, "Iffdetector: inference-aware feature filtering for object detection," *IEEE Trans. Neural Netw. Learn. Syst.*, vol. 33, no. 11, pp. 6494–6503, 2021.
- [15] D. Qi, J. Hu, and J. Shen, "Few-shot object detection with self-supervising and cooperative classifier," *IEEE Trans. Neural Netw. Learn. Syst.*, 2023.
- [16] Z. Tian, C. Shen, H. Chen, and T. He, "Fcos: Fully convolutional one-stage object detection," in *Proc. ICCV*, 2019, pp. 9627–9636.
- [17] C. Feng, Y. Zhong, Y. Gao, M. R. Scott, and W. Huang, "Tood: Task-aligned one-stage object detection," in *Proc. ICCV*, 2021, pp. 3490–3499.
- [18] Y. Wu, Y. Chen, L. Yuan, Z. Liu, L. Wang, H. Li, and Y. Fu, "Rethinking classification and localization for object detection," in *Proc. CVPR*, 2020, pp. 10186–10195.
- [19] Z. Yang, S. Liu, H. Hu, L. Wang, and S. Lin, "Reppoints: Point set representation for object detection," in *Proc. ICCV*, 2019, pp. 9657–9666.
- [20] X. Zhang, F. Wan, C. Liu, R. Ji, and Q. Ye, "Freeanchor: Learning to match anchors for visual object detection," in *Proc. NIPS*, vol. 32, 2019.
- [21] X. Dai, Y. Chen, B. Xiao, D. Chen, M. Liu, L. Yuan, and L. Zhang, "Dynamic head: Unifying object detection heads with attentions," in *Proc. CVPR*, 2021, pp. 7373–7382.
- [22] G. Song, Y. Liu, and X. Wang, "Revisiting the sibling head in object detector," in *Proc. CVPR*, 2020, pp. 11563–11572.
- [23] J. Dai, H. Qi, Y. Xiong, Y. Li, G. Zhang, H. Hu, and Y. Wei, "Deformable convolutional networks," in *Proc. ICCV*, 2017, pp. 764–773.
- [24] T.-Y. Lin, M. Maire, S. Belongie, J. Hays, P. Perona, D. Ramanan, P. Dollár, and C. L. Zitnick, "Microsoft coco: Common objects in context," in *Proc. ECCV*. Springer, 2014, pp. 740–755.
- [25] Z. Liu, Y. Lin, Y. Cao, H. Hu, Y. Wei, Z. Zhang, S. Lin, and B. Guo, "Swin transformer: Hierarchical vision transformer using shifted windows," in *Proc. ICCV*, 2021, pp. 10012–10022.
- [26] J. Deng, W. Dong, R. Socher, L.-J. Li, K. Li, and L. Fei-Fei, "Imagenet: A large-scale hierarchical image database," in *Proc. CVPR*. Ieee, 2009, pp. 248–255.
- [27] Z.-Q. Zhao, P. Zheng, S.-t. Xu, and X. Wu, "Object detection with deep learning: A review," *IEEE Trans. Neural Netw. Learn. Syst.*, vol. 30, no. 11, pp. 3212–3232, 2019.



- [28] Y. Liu, D. Zhang, Q. Zhang, and J. Han, "Part-object relational visual saliency," *IEEE Trans. Pattern Anal. Mach. Intell.*, vol. 44, no. 7, pp. 3688–3704, 2021.
- [29] Y. Liu, D. Cheng, D. Zhang, S. Xu, and J. Han, "Capsule networks with residual pose routing," *IEEE Trans. Neural Netw. Learn. Syst.*, 2024.
- [30] R. Girshick, "Fast r-cnn," in *Proc. ICCV*, 2015, pp. 1440–1448.
- [31] S. Ren, K. He, R. Girshick, and J. Sun, "Faster r-cnn: Towards real-time object detection with region proposal networks," in *Proc. NIPS*, vol. 28, 2015.
- [32] Z. Cai and N. Vasconcelos, "Cascade r-cnn: Delving into high quality object detection," in *Proc. CVPR*, 2018, pp. 6154–6162.
- [33] J. Hu, L. Shen, and G. Sun, "Squeeze-and-excitation networks," in *Proc. CVPR*, 2018, pp. 7132–7141.
- [34] R. Yang, L. Song, Y. Ge, and X. Li, "Boxsnake: Polygonal instance segmentation with box supervision," *arXiv preprint arXiv:2303.11630*, 2023.
- [35] G. Xu, C. He, H. Wang, H. Zhu, and W. Ding, "Dm-fusion: Deep model-driven network for heterogeneous image fusion," *IEEE Trans. Neural Netw. Learn. Syst.*, 2023.
- [36] J. Yao, X. Pan, T. Wu, and X. Zhang, "Building lane-level maps from aerial images," in *Proc. ICASSP*. IEEE, 2024, pp. 3890–3894.
- [37] M. Gao, F. Zheng, J. J. Yu, C. Shan, G. Ding, and J. Han, "Deep learning for video object segmentation: a review," *Artificial Intelligence Review*, vol. 56, no. 1, pp. 457–531, 2023.
- [38] Z. Shao, J. Han, K. Debatista, and Y. Pang, "Textual context-aware dense captioning with diverse words," *IEEE Trans. Multimedia*, 2023.
- [39] J. Yao, C. Li, K. Sun, Y. Cai, H. Li, W. Ouyang, and H. Li, "Ndc-scene: Boost monocular 3d semantic scene completion in normalized device coordinates space," in *Proc. ICCV*. IEEE Computer Society, 2023, pp. 9421–9431.
- [40] A. Dosovitskiy, L. Beyer, A. Kolesnikov, D. Weissenborn, X. Zhai, T. Unterthiner, M. Dehghani, M. Minderer, G. Heigold, S. Gelly *et al.*, "An image is worth 16x16 words: Transformers for image recognition at scale," *arXiv preprint arXiv:2010.11929*, 2020.
- [41] R. Yang, H. Ma, J. Wu, Y. Tang, X. Xiao, M. Zheng, and X. Li, "Scalablevit: Rethinking the context-oriented generalization of vision transformer," in *Proc. ECCV*. Springer, 2022, pp. 480–496.
- [42] F. Li, H. Zhang, S. Liu, J. Guo, L. M. Ni, and L. Zhang, "Dn-detr: Accelerate detr training by introducing query denoising," in *Proc. CVPR*, 2022, pp. 13 619–13 627.
- [43] H. Duan, Y. Long, S. Wang, H. Zhang, C. G. Willcocks, and L. Shao, "Dynamic unary convolution in transformers," *IEEE Trans. Pattern Anal. Mach. Intell.*, 2023.
- [44] Z. Shao, J. Han, D. Marnierides, and K. Debatista, "Region-object relation-aware dense captioning via transformer," *IEEE Trans. Neural Netw. Learn. Syst.*, 2022.
- [45] H. Zhou, L. Tang, R. Yang, G. Qin, Y. Zhang, R. Hu, and X. Li, "Uniqua: Unified vision-language pre-training for image quality and aesthetic assessment," *arXiv preprint arXiv:2406.01069*, 2024.
- [46] J. Yao, T. Wu, and X. Zhang, "Improving depth gradient continuity in transformers: A comparative study on monocular depth estimation with cnn," *arXiv preprint arXiv:2308.08333*, 2023.
- [47] A. Hatamizadeh, H. Yin, G. Heinrich, J. Kautz, and P. Molchanov, "Global context vision transformers," in *Proc. ICML*. PMLR, 2023, pp. 12 633–12 646.
- [48] W. Wang, E. Xie, X. Li, D.-P. Fan, K. Song, D. Liang, T. Lu, P. Luo, and L. Shao, "Pyramid vision transformer: A versatile backbone for dense prediction without convolutions," in *Proc. ICCV*, 2021, pp. 568–578.
- [49] J. Ho, N. Kalchbrenner, D. Weissenborn, and T. Salimans, "Axial attention in multidimensional transformers," *arXiv preprint arXiv:1912.12180*, 2019.
- [50] Z. Huang, X. Wang, L. Huang, C. Huang, Y. Wei, and W. Liu, "Ccnet: Criss-cross attention for semantic segmentation," in *Proc. ICCV*, 2019, pp. 603–612.
- [51] X. Dong, J. Bao, D. Chen, W. Zhang, N. Yu, L. Yuan, D. Chen, and B. Guo, "Cswin transformer: A general vision transformer backbone with cross-shaped windows," in *Proc. CVPR*, 2022, pp. 12 124–12 134.
- [52] X. Zhu, H. Hu, S. Lin, and J. Dai, "Deformable convnets v2: More deformable, better results," in *Proc. CVPR*, 2019, pp. 9308–9316.
- [53] Q. Wan, Z. Huang, J. Lu, G. Yu, and L. Zhang, "Seaformer: Squeeze-enhanced axial transformer for mobile semantic segmentation," *arXiv preprint arXiv:2301.13156*, 2023.
- [54] X. Chu, Z. Tian, B. Zhang, X. Wang, X. Wei, H. Xia, and C. Shen, "Conditional positional encodings for vision transformers," *arXiv preprint arXiv:2102.10882*, 2021.
- [55] L. H. Li, P. Zhang, H. Zhang, J. Yang, C. Li, Y. Zhong, L. Wang, L. Yuan, L. Zhang, J.-N. Hwang *et al.*, "Grounded language-image pre-training," in *Proc. CVPR*, 2022, pp. 10 965–10 975.
- [56] M. Everingham, L. Van Gool, C. K. Williams, J. Winn, and A. Zisserman, "The pascal visual object classes (voc) challenge," *Int. J. Comput. Vis.*, vol. 88, pp. 303–338, 2010.
- [57] K. Chen, J. Wang, J. Pang, Y. Cao, Y. Xiong, X. Li, S. Sun, W. Feng, Z. Liu, J. Xu *et al.*, "Mmdetection: Open mmlab detection toolbox and benchmark," *arXiv preprint arXiv:1906.07155*, 2019.
- [58] X. Li, W. Wang, X. Hu, J. Li, J. Tang, and J. Yang, "Generalized focal loss v2: Learning reliable localization quality estimation for dense object detection," in *Proc. CVPR*, 2021, pp. 11 632–11 641.
- [59] S. Li, C. He, R. Li, and L. Zhang, "A dual weighting label assignment scheme for object detection," in *Proc. CVPR*, 2022, pp. 9387–9396.
- [60] Z. Chen, C. Yang, J. Chang, F. Zhao, Z.-J. Zha, and F. Wu, "Ddod: Dive deeper into the disentanglement of object detector," *IEEE Trans. Multimedia*, 2023.
- [61] S. Liu, F. Li, H. Zhang, X. Yang, X. Qi, H. Su, J. Zhu, and L. Zhang, "Dab-detr: Dynamic anchor boxes are better queries for detr," *arXiv preprint arXiv:2201.12329*, 2022.
- [62] S. Zhang, X. Wang, J. Wang, J. Pang, C. Lyu, W. Zhang, P. Luo, and K. Chen, "Dense distinct query for end-to-end object detection," in *Proc. CVPR*, 2023, pp. 7329–7338.
- [63] Y. Chen, Z. Zhang, Y. Cao, L. Wang, S. Lin, and H. Hu, "Reppoints v2: Verification meets regression for object detection," in *Proc. NIPS*, vol. 33, 2020, pp. 5621–5631.
- [64] P. Sun, R. Zhang, Y. Jiang, T. Kong, C. Xu, W. Zhan, M. Tomizuka, L. Li, Z. Yuan, C. Wang *et al.*, "Sparse r-cnn: End-to-end object detection with learnable proposals," in *Proc. CVPR*, 2021, pp. 14 454–14 463.
- [65] F. Gao, Y. Cai, F. Deng, C. Yu, and J. Chen, "Feature alignment in anchor-free object detection," *IEEE Trans. Circuits Syst. Video Technol.*, 2023.
- [66] X. Zhu, W. Su, L. Lu, B. Li, X. Wang, and J. Dai, "Deformable detr: Deformable transformers for end-to-end object detection," *arXiv preprint arXiv:2010.04159*, 2020.
- [67] K. He, G. Gkioxari, P. Dollár, and R. Girshick, "Mask r-cnn," in *Proc. ICCV*, 2017, pp. 2961–2969.
- [68] K. Chen, J. Pang, J. Wang, Y. Xiong, X. Li, S. Sun, W. Feng, Z. Liu, J. Shi, W. Ouyang *et al.*, "Hybrid task cascade for instance segmentation," in *Proc. CVPR*, 2019, pp. 4974–4983.
- [69] J. Zhao, L. Sun, and Q. Li, "Recursive-detr: end-to-end region-based recursive object detection," in *Proc. ICCV*, 2023, pp. 6307–6316.